

Technical Impacts of Light-Duty and Heavy-Duty Transportation Electrification on a Coordinated Transmission and Distribution System

Farnaz Safdarian*, Diana Wallison*, Jessica L. Wert,
Oluwatoyin Oshinkoya, Jung Kyo Jung, Thomas J. Overbye
Department of Electrical and Computer Engineering
Texas A&M University
College Station, TX
{fsafdarian, diwalli, jwert, toyin_21, jjungkyo, overbye}@tamu.edu

Yanzhi Xu
ElectroTempo
Arlington, VA
ann.xu@electrotempo.com

Abstract—In this paper, we propose a strategy to model the required spatio-temporal charging demand from light-duty (LD) and medium- and heavy-duty (MHD) electric vehicles (EVs) using actual transportation data by mapping the demand for the required EV charging to a realistic and coordinated distribution and transmission electric grid at the predicted times of the day to study their impact on power system in a variety of load, weather and EV penetration scenarios. This work is the first study that includes the actual weather data and transportation data with realistic and coordinated distribution and transmission grid data in a large industry-scale level study. The main goal of this study is to identify possible issues and required upgrades in the electric grid, caused by an increase in EV integration. The transmission case study is a large grid with 6717 buses over Texas footprint and the distribution grid is over Houston, a city in Texas, covering over 3 million customers. The resulting overloads and voltage violations experienced in the system are discussed and required planning upgrades to avoid these issues are suggested.

Index Terms—Electrification, Electric Vehicles, Trucks, Transportation, Transmission, Distribution, Charging, ac Optimal Power Flow

I. INTRODUCTION

As electric power generation through renewable energy resources increases, electric vehicles (EVs) are considered as a key technology to control oil usage and to achieve net-zero emissions in the road transportation sector. According to BloombergNEF (a strategic research provider covering global commodity markets and the disruptive technologies driving the transition to a low-carbon economy), light-duty (LD) EV sales are anticipated to increase steeply in the coming years, with an estimated rise from 3 million in 2020 to 14 million in 2025 all over the world [1]. It is estimated that global sales of EVs grow by 39% year to year while the overall sale of conventional cars was reduced by up to 14% in 2020. Also, it is predicted that EV sales will increase up to 30 million in 2028 and will represent roughly 50% of new car sales in

2030 [2]. Further, California recently passed legislation to ban LD internal combustion vehicle sales by 2035 [3], putting the state on a more rapid sales curve than [2]. Using an established vehicle adoption model [4], a sales curve according to California’s legislation will result in about 20% of the LD vehicle population being EVs by 2029. For medium- and heavy-duty (MHD) EV penetration, reference [5] estimates that around 7% of MHD vehicles in operation will be EV by 2030. Reference [6] finds that by 2030 MHD market share is between 4% and 8% in a business as usual scenario, and between 8% to 25% under a more policy-aggressive scenario. For policy, United States Environmental Protection Agency [7] proposed to reduce harmful emissions and promote the increase of MHD EV penetration.

Both transportation and power sectors should be ready to adjust to these changes. From the transportation side, sufficient charging lots including public charging lots and home charging stations should be available to facilitate EV charging and achieving electrification. From the electrical grid side, the infrastructure of both transmission and distribution grids should also be ready for this increase in the EVs’ charging demand. Therefore, a coordinated study between the transportation infrastructure, transmission grid and distribution grid is required and the study must include realistic data.

In order to study the impact of the EVs on the grid, it is crucial to study a variety of possible EV penetration scenarios in a variety of load and weather scenarios. Historically, weather information has only been indirectly included in the operation problems as the outputs of renewable resources are used as input to the ac optimal power flow (OPF) problems. [8] However, with the growth in the penetration of renewable resources, the dependency of the OPF on the weather measurements has grown substantially and major power system input parameters such as wind and solar generator capacities are more weather dependent. Therefore, it is crucial for power system studies to provide a consistent and feasible way to set these many weather-dependent values online based on the weather changes, in a way that the inclusion of weather measurements

in an OPF data file has little impact on the file size and does not require substantial changes to existing algorithms. This would be direct inclusion of weather measurements gathered from thousands of weather stations all over the world to the OPF problems based on mapping them to the closest buses to update real-time available capacities of all generators based on the weather measurements. There are very few papers that directly include the impact of weather in the OPF. Reference [9] introduces a weather-based OPF algorithm with wind farm integration by considering the temperature-related resistance and dynamic line rating of overhead transmission lines on small case studies with up to 39 buses. However, the proposed strategy is not easily extendable and implementable on large-scale grids. This paper uses a strategy for direct inclusion of weather in the ac OPF introduced in our previous work [10].

A. Literature Review

Some references in the literature focus on coupling transportation systems with the electrical grid. Reference [11] reviews various methods for coupling power system distribution and transportation grids and investigates the impact of EVs on these integrated systems. Reference [12] studies the effects of EV charging facilities on the electric distribution system and explores strategies to enhance system stability and efficiency in integrated electrified transportation systems using charging control methods. Then works [13] and [14] introduce a transmission-distribution dynamic co-simulation framework and analyze the influence of EVs on system frequency regulation. References [15] and [16] investigate the impact of EV charging on electric power distribution systems, considering single-phase rooftop solar photovoltaic (PV) systems. Reference [17] explores the impact of EVs on power distribution systems, focusing on stability and efficiency.

Charging infrastructures are an important obstacle to electrifying the whole market and the current EV charging lots in most parts of the world are not enough for a convenient transportation electrification. Reference [18] studies the optimal placement of EV charging stations in the distribution network, and work [19] proposes a multi-objective planning model that simultaneously considers the role of fast charging stations and their locations in the electrical and transportation sectors.

The power grid limitations and capacities including generation capacity and line capacities is another obstacle for transportation electrification that should be studied carefully. Reference [20] introduces a case study for transportation electrification in Abu Dhabi using a transportation system topology, an electric power topology, and EV charging demand. However, the case study is just a distribution system and the connected transmission grid is ignored. Reference [21] claims that the electricity distribution grid infrastructure is not ready for even 10% EV penetration. However, the proposed charging pattern that is studied in [21] is an uncoordinated EV charging demand in the residential sector and not the most possible charging pattern. We have studied three possible charging patterns in our previous work [22], and selected the most

possible pattern then modeled and studied the spatio-temporal impact of LD and MHD EVs in operational emissions in [23].

On the other hand, study [24] shows heavy-duty EVs do not create major overloading issues on the distribution system studying 36 distribution substations in Texas, United States while each fleet is limited to 100 EVs with charging capacity of 100 kW assuming that their short, predictable routes and return-to-base applications, allow these heavy-duty EVs to recharge when off shift at their depots. However, this should be studied with a more realistic EV penetration of both LD and MHD EV demand, and on a larger, coordinated distribution and transmission grid. Therefore, the current literature lacks a detailed and comprehensive study on the resiliency of the current grid to significant levels of EV integration to conclude the contradictory results and suggest upgrades to avoid power system operation issues.

B. Contributions

Whether the electrical grid is ready for electrifying transportation or not depends on factors such as the electric grid structure, parameters and capacities of devices, charging patterns, amount of charging demand as well as weather and load at each time. Therefore, we perform a comprehensive study based on real transportation data on a large industry-scale grid and coordinated the distribution and transmission grids over a variety of load, EV penetration and weather scenarios for power system planning to make sure that the grid will adjust to larger penetrations of EVs and avoid major reliability issues. We propose a detailed strategy to model the possible spatio-temporal charging demands of LD and MHD EVs using actual transportation data and map the demand for the required EV charging to a realistic distribution and transmission electric grid at the predicted times of the day. This work is the first study that includes the actual weather data and transportation data with realistic and coordinated distribution and transmission grid data in a large industry-scale level study. After the proposed modelling is performed on a case study over Texas, US footprint, AC optimal power flow simulations are run, problematic points of the grid are found and required planning upgrades to avoid any line overload or voltage issue are suggested.

In summary, the main contributions of this paper are:

- Creating a coupled-infrastructure model of a transportation network, realistic transmission and distribution coordinated grids data
- Estimating a detailed spatial and temporal realistic and common charging data with behaviorally-informed charging patterns that consider the anxiety level of drivers and EV types and mapping it to a large-scale, realistic and coordinated distribution and transmission grid
- Showing the importance of direct inclusion of weather data (varying with location and time) in power system models when quantifying charging demand and study ac OPF to determine and propose required system upgrades based on an increase in the penetration of EVs in the

transportation sector in a variety of load and weather scenarios

II. MODELING EV CHARGING DEMAND

A. Modeling EV Charging Demand

1) *Traffic Modeling*: The traffic modeling used in this paper is performed using the regional Travel Demand Model (TDM). TDMs are typically used in the regional transportation planning process. The TDM contains information about trips including origins and destinations with their exact geographical coordinates, vehicle type, trip distances, duration, and speeds for various time periods in a typical day. The information from the TDM is used to estimate the on-road energy consumption of vehicles.

2) *EV Charging Load Modeling*: The key linkage between the transportation system and power system is spatio-temporal charging demand. Considering the critical importance of a realistic charging pattern, we constructed a realistic charging demand strategy considering the original travel model for trip origins and destinations, a vehicle dynamics model for EV energy consumption, and used surveys on travel and charging behaviours.

The trip duration and ending locations are determined using survey data containing personal interviews to measure and identify travel patterns of vehicles entering and exiting a particular study area [25]. The overall charging demand at these locations is calculated using the trip data mileage, vehicle registration data, and vehicle emissions data [26]. First, all trips are divided into those performed by automobiles and trucks and then model vehicle attributes are used as a key to estimating the energy consumption of each trip, such as vehicle class and type. Trip attributes are considered to assign the associated demand to specific times and locations in the transportation network. These vehicle and trip attributes are modeled separately for light duty (LD) vehicles and medium and heavy duty (MHD) vehicles to reflect the different EV markets, charging behavior, and charging locations. Then, energy usage associated with each trip is estimated and hourly charging demand within the transportation network is assigned according to these predicted vehicle and trip attributes and modeled vehicle miles traveled. Markov chain Monte Carlo (MCMC) [27] is used to model uncertainties.

For every LD EV trip, a vehicle type and its associated range, battery capacity, and estimated energy consumption per mile is generated based on historical data. Three different types of LD EVs are considered to represent variation within the market: vehicles can have a range of 100, 200 and 300 miles and energy consumption rates per mile from 0.27 kWh per mile to 0.34 kWh per mile. Reference [28] is used to estimate these energy consumption rates. For every household in the travel demand model, using penetration rate and market share, the specific portion of available household vehicles are randomly designated as EVs. Each person in the household may be associated with a set of tours (a chain of trips that begin and end at home, with stops in between); we assign available EVs in each household to the longest tours. It is

assumed that for home charging LD EVs, level 1 chargers with 120 V and a maximum current of 12 amps are used. This corresponds to a power output of approximately 1.4 kW. It is also assumed EVs start the first trip of the day with a full charge. The public charging, workplace charging, and home charging are modeled separately using different charging logics. Our charging logic assumptions are based on surveys [29]–[31] and are considered the dominant charging pattern for LD EVs, which is to favor home charging. We characterize public charging as energy demanded from trips that do not start at home and have a non-work trip purpose. If the trip energy requirement would bring the vehicle below a certain state of charge, it would be willing to charge between trips in a tour, (even if stop duration would allow a partial refill) we assume it will charge using fast chargers at 100 kW. The threshold for charging (range anxiety) is also treated as a random variable with a gamma distribution to account for diversity in travelers' behavior. We use a stated preference survey to estimate the parameters of this distribution. The mean range anxiety is estimated 32.9 miles. The estimated public charging demand is a function of that vehicle's consumption rate and the mileage of the previous trip. If a trip is modeled to end at workplace, we assign all charging demand to that trip end as workplace charging and we assume the vehicle charges to full at 19 kW. Finally, we assume the vehicle charges overnight to full at 2.4 kW immediately after arrival at home (the end time of the last trip of the day). The random generation of EVs by household, assignment of EV types to trips, and the resulting energy demand assignment within the network are repeated to produce an average estimate of charging demand. Our other assumptions are that the first trip of the day probability is not correlated with location; distance traveled is not correlated with location or EV type; and that range anxiety is not correlated with time, location, or EV type.

For MHD EVs, this paper considers short-haul MHD vehicles with the range of 350 miles charging at their depots. We assume that the MHD vehicles are charged with 100 kW level 3 (fast) chargers. The fast-charging demand forecasting model based on a data-driven approach and human decision-making behavior is presented in more detail in [32]. The human behavior decision-making model is based on Regret Theory [33], [34], equation (1), which comprises the utility of time consumption and charging cost to plan driving paths and recommend fast-charging stations for vehicles.

$$R_i = \sum_{j=1} \sum_{m=1 \dots M} \ln[1 + e^{\beta_m * (X_{jm} - X_{im})}] \quad (1)$$

β_m are attribute weights for driver decisions on charging. $X_{i,m}$ and $X_{j,m}$ refer to the decisions i and j , where i is to charge the EV and j is to postpone charging and m is the battery state of charge.

Also, commercial vehicle data are used to estimate the required charging locations of MHD EVs. [28] The rules obtained from data mining together with established models are combined to construct the 'Electric Vehicles–Power

Grid-Traffic Network' fusion architecture. A key innovation of this simulation is the depot probability model. Nearly 1,000 individually labeled land parcels using satellite imagery are used for training. We applied this model to every land parcel in the region and predicted its probability of being a depot. Without this step, it would not be possible to identify places in the transportation network where a large truck would be eligible to charge, as they typically cannot make use of public charging infrastructure designed for LD EVs. This model reflects the complex correlation structure between numerous attributes of vehicle trips, including vehicle class and type, fuel type, cargo type, origin county, trip time of day, and whether the trip is the first or last of the day. The last element, whether a trip is the last of the day, determines the assumed charging behavior. After the last trip of the day, we assume trucks will charge overnight, or as much as possible before the predicted time of the first trip of the next day. For mid-day trips, we assign charging demand based on the mileage of the trip and the energy consumption rate of the truck. The estimated energy consumption from mid-day trips (trips that are not the last of the day) that end within 100 meters of a predicted truck depot is assigned to the node nearest to that depot. The demand that is unmet during the day because the trip does not end near a depot is proportionately distributed to all nodes that do contain depots as overnight charging.

Note that using trips as the building block for our simulation upholds a key principle of travel demand modeling: that travel (and thus, the associated energy demand) is derived from the demand for activities such as working, vacationing, shopping, or commerce. Regardless of the predominant vehicle power-train technology, the need to participate in these day-to-day activities persists. Given the dearth of empirical or prospective (stated preference) evidence on this matter, and that these speculative behavioral shifts are influenced by many social, environmental, and economic factors beyond EV adoption, we use current vehicle travel data without further adjustment. The EV charging demand described is represented mathematically by equation (2). Where E_i is the charging amount in kWh for hour i . n_i is the number of EV trips according to the EV adoption level simulated using the Markov Chain model described in [35]. NHC_{ij} is a binary variable indicating whether non-home charging is occurring, based on surveys and Regret Theory. NHE_{ij} is the amount of non-home charging in kWh calculated by multiplying the distance traveled by the vehicle energy consumption rate [32]. HC_{ij} is a binary variable indicating whether home charging is occurring. HE_{ij} refers to the amount of home charging in kWh. UHC refers to unfinished home charging of last trips ended before hour h , equation (3).

$$E_i = \sum_{j=1}^{n_i} (NHC_{ij} * NHE_{ij} + HC_{ij} * HE_{ij}) + UHC \quad (2)$$

for $i > 1$

$$UHC = \sum_{i=1}^{h-1} \sum_{j=1}^{n_x} HE_{ij} \quad (3)$$

Using the proposed strategy, hourly charging demand L_{LD} L_{MHD} for LD and MHD vehicles based on their percentage is calculated from Equations (5) and (4). These equations show the mathematical model for the charging demand from LD and MHD EVs for a sample average day where X is the hour of the day. M_1 is the multiplier used to represent the EV penetration percentage of LD vehicles and M_2 is the EV penetration percentage for MHD vehicles. This model gives an approximation of the required charging demand based on the type and EV penetration.

$$L_{LD} = M_1(0.023X^5 - 1.66X^4 + 45.29X^3 - 506.3X^2 + 1607X + 4747.1) \quad (4)$$

$$L_{MHD} = M_2(0.0009X^6 - 0.066X^5 + 1.88X^4 - 25.57X^3 + 169.51X^2 - 521.61X + 930.53) \quad (5)$$

B. Mapping EV Load to the Distribution System

With information on geographical coordinates of the charging demand and geographic topology of the electric grid, the EV charging loads are mapped to the appropriate distribution-level nodes using the mapping methodology developed in our previous work [36]. The mapping takes the latitudes and longitudes of nodes in the distribution system and creates tessellating service areas using a Voronoi diagram. The nodes are centrally-located within their respective service territories. As this work includes distribution grid simulation, the service areas are needed at the distribution system level, which is connected to the transmission grid.

The process of this mapping for purely distribution-level simulation is as follows:

- 1) Using the geographic feeder node coordinates, create a Voronoi diagram to represent the division of service areas for each distribution feeder node.
- 2) For each EV charging station, determine the feeder node corresponding to the service area in which the charging station lies.
- 3) Include a load in the electric grid model to represent the aggregate EV charging stations within the service area.

C. Load Time Series

Once the load from each EV charger is mapped to its feeder node within the distribution system, the EV load time series developed in Section II-A is represented as a load at the appropriate nodes in the system. The estimated EV charging demand is then added to the spatio-temporal load of the base case. The grid base load (all load excluding the load related to EV charging) of distribution grid at each feeder is created based on the approach described in [37], which

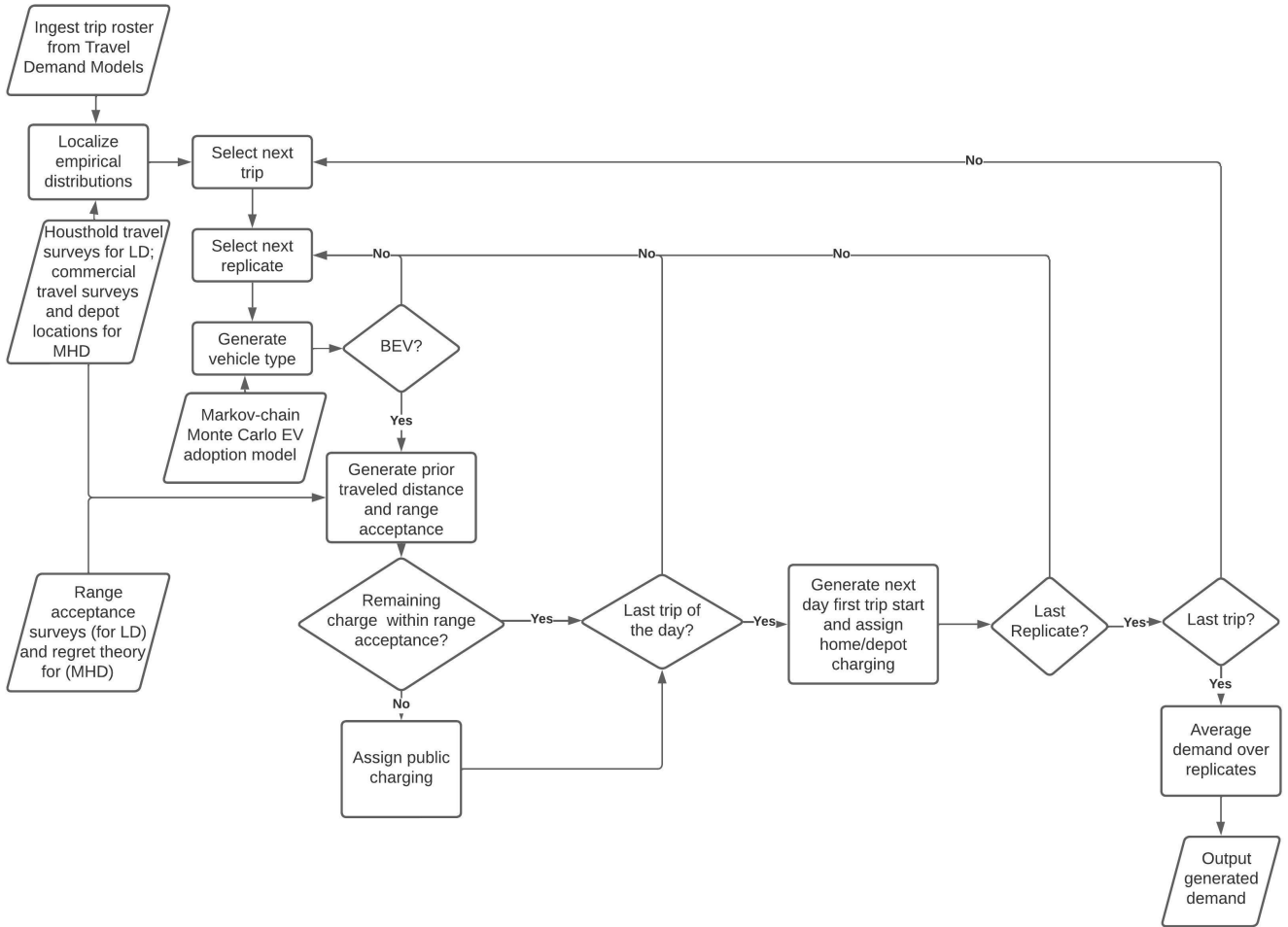


Fig. 1: Flowchart of the process of creating LD and MHD EV charging demand

uses ResStock and ComStock tools. Each feeder is assigned a ResStock and ComStock profile based on customer type and peak load. The transmission grid base load is created for the base case using the approach outlined in [38]. This approach develops bus-level load time series using data on the residential, commercial, and industrial (RCI) ratio and sample building-level load curves from similar geographic locations. The integration process is generalized and also improved by taking aggregation effects into consideration. The maximum value of the load time series aims to match the corresponding load bus size determined in the base case. The unique variation of each bus-level time series is a result of the heuristic aggregation of prototypical building and facility load time series.

III. CO-SIMULATION

A. Co-Simulation Framework

The distribution and transmission networks, used in the study, are connected and coordinated to study the effects of EV charging on overall system reliability. The ac OPF of the combined system is calculated by first calculating the ac OPF for

the distribution network and then for the transmission system. The voltage magnitude and angle, of the 69kV buses, alongside their real and reactive loads are the shared variable between transmission and distribution systems. These values from the results of ac OPF are then used to initialize the ac OPF for the transmission network. At each time step the shared variables for both systems are sent to a controller which determines if the two systems have converged to a shared optimal solution. If convergence is not achieved, the results for the shared variables of the transmission network are used as inputs for the distribution side of the co-simulation and a new distribution level ac OPF solution is calculated. Respectively, the results for the shared variables of the distribution network are used as inputs for the transmission side of the co-simulation and a new transmission ac OPF solution is calculated. This process continues, iteratively, until the controller achieves convergence between the two systems.

B. AC Optimal Power Flow (AC-OPF)

AC-OPF [39] is solved to determine the steady-state output power of generators, power flowing between the lines, and

voltage outputs of buses in the distribution and transmission power system in a way to minimize the operation cost and satisfy the power grid constraints. Coefficients (a , b , and c) that represent quadratic cost curve elements of generators specify $\mathcal{F}_c(P_G)$:

$$\min_{P_G} \mathcal{F}_c(P_G) = \sum_{g=1}^{|\mathcal{G}|} [a_g + b_g P_{G,g} + c_g P_{G,g}^2] \quad (6)$$

Equation (6) is the objective function of the ac OPF and the constraints including active and reactive power balance equations (7, 8) as well as additional operational constraints equation from (9) to (12) should be satisfied. [39].

$$P_{G,(g \in \mathcal{G}(i))} - P_{D,i} = |V_i| \sum_{k=1}^{|N|} |V_k| (G_{ik}^Y \cos \theta_{ik} + B_{ik}^Y \sin \theta_{ik}) \quad (7)$$

$$Q_{G,(g \in \mathcal{G}(i))} - Q_{D,i} = |V_i| \sum_{k=1}^{|N|} |V_k| (G_{ik}^Y \sin \theta_{ik} - B_{ik}^Y \cos \theta_{ik}) \quad (8)$$

$$P_{min,g} \leq P_{G,g} \leq P_{max,g} \quad \forall g \in \mathcal{G} \quad (9)$$

$$Q_{min,g} \leq Q_{G,g} \leq Q_{max,g} \quad \forall g \in \mathcal{G} \quad (10)$$

$$V_{min,i} \leq |V_i| \leq V_{max,i} \quad \forall i \in \mathcal{N} \quad (11)$$

$$P_l^2 + Q_l^2 \leq S_{max,l}^2 \quad \forall e \in \mathcal{E} \quad (12)$$

A voltage magnitude is represented by $|V_i|$ at the i^{th} bus, and a voltage angle is indicated by θ_i variable at the i^{th} bus in the equations. That voltage angle of the i^{th} subtracts one of k^{th} buses is the θ_{ik} . In this case, N is the amount of buses in the system. Individually, $P_{D,i}$ and $Q_{D,i}$ express as the real and reactive power demands at the i^{th} bus as well as $P_{G,g}$ and $Q_{G,g}$ also express as real and reactive power generation of the g^{th} generator. It is noticeable that \mathcal{G} is the amount of all generators in the system. The bus admittance matrix is expressed by as a real part G_{ik}^Y , and an imaginary part B_{ik}^Y . Maximum as well as minimum operating limits in the generator are supplied by $(P_{min,g}, P_{max,g})$ for real power, and $(Q_{min,g}, Q_{max,g})$ for reactive power. $(V_{min,i}, V_{max,i})$ are limited in voltage magnitude of each bus. The power flow of the branch, l , is its thermal limit, also $S_{max,e}$ is involved in real and reactive power flow in equation (12). The power flow of the branches including lines and transformers in the grid are calculated in equations (13-14). It should be noted that \mathcal{E} is the number of all branches in the power system.

$$P_l = |V_i|^2 G_{ik}^Y - |V_i| |V_k| (G_{ik}^Y \cos \theta_{ik} + B_{ik}^Y \sin \theta_{ik}) \quad (13)$$

$$Q_l = -|V_i|^2 B_{ik}^Y - |V_i| |V_k| (B_{ik}^Y \cos \theta_{ik} - G_{ik}^Y \sin \theta_{ik}) \quad (14)$$

TABLE I:
Acceptable Multipliers of Nameplate Rating

Ratings	Winter	Summer
Normal	1.23	1.1
Emergency – 15 minutes	1.83	1.67
Emergency – 4 hours	1.34	-
Emergency – 12 hours	-	1.18

C. Network Constraints

As mentioned in the previous section, Equations (13-14) show how to calculate the real and reactive power flowing in each branch and each branch has a limited apparent power transfer capacity shown by Equation (12). Based on North American Electric Reliability Cooperation (NERC) standards on system operating limit and exceedance clarification, a 24-hour continuous line rating is an example of a normal rating; however, rating practices vary from entity to entity and may include ratings that vary with ambient temperature. Typical short-term Emergency Ratings (around 10% of line capacity) have a finite duration of less than 24 hours (usually 4 hours for winter emergency and 12 hours for summer) and short-term emergency rating (around 15% of line capacity) is usually acceptable just for 15 minutes [40], [41]. The ratings given in Table I are based on American National Standards Institute (ANSI) C37.010 limits. The line overloads in the grid that are greater than the acceptable normal or emergency MVA ratings and last for a longer duration than the defined standards, can create major reliability issues.

D. Direct Inclusion of Weather Data

Since the available capacities and output power of renewable energy resources such as wind turbines and solar power plants is directly related to the weather conditions, weather measurements are directly included in the power flow modeling, according to the strategy outlined in [10]. Unlike conventional methods that rely on output from renewable generators at utility scale, this technic incorporates direct weather data, enhancing the precision of individual renewable generation estimates and tracking sudden weather changes more effectively. Also, using direct inclusion of weather data in ac OPF problems, a wide variety of historical weather scenarios can be studied in a specific grid and generation mix.

Detailed weather measurements such as wind speed and wind direction at surface, wind speed and wind direction at 100 meter height, cloud coverage percentage, radiations, temperatures and dew points are extracted from the International Civil Aviation Organization (ICAO) [42], the World Meteorological Organization (WMO) [43], and European Centre for Medium-Range Weather Forecasts (ECMWF) Re-Analysis, fifth generation (ERA5) [44] on an hourly basis from 1940 to the current date.

Then this data is mapped with generators based on geographic proximity. Detailed data of renewable generator models and power curves in United States are used from U.S. Energy Information Administration website form EIA-860 [45]. To assess weather impacts on renewable generators, six models

are developed. The first to fourth model, referencing [46], [47], [48] and [49], estimate wind power plant output using wind data and wind turbine power curves based on their types. The fifth model uses local solar data and configurations from [46] for solar PV output projection, while the sixth model, informed by [50], predicts thermal generator output changes due to temperature variations. The results are validated in [51] and [52]. In the next step, to find the optimal dispatch of conventional generators and flow in the lines considering reactive power limitations, an ac OPF is solved.

IV. CASE STUDY

The study requires access to realistic distribution and transmission grid data. This is often difficult as electric grid data is considered Critical Energy/Electric Infrastructure Information (CEII) marking it as restricted. To circumvent this issue, we have used synthetic grids built over Texas, United States. The full system used for the case, includes a transmission system supplying the entirety of Texas, United States, and a distribution system that supplies specifically Houston, Texas, a diagram showing the two systems is illustrated in Fig. 2. This allows us access to realistic data for a transmission and distribution grid over certain geographic coordination footprint without disclosing any CEII.

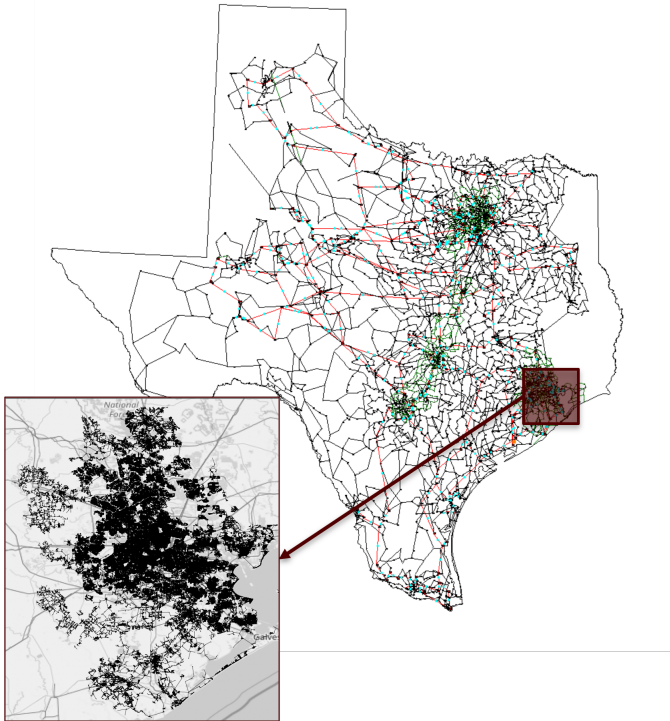


Fig. 2: Combined transmission and distribution system

A. Distribution System

The synthetic distribution network is created using the process outlined in [37] based on the U.S. Reference Network Model tool (RNM-US). This approach uses land parcel data

[53], and a catalog of technical parameters obtained from commercial and open source data [54] to create realistic synthetic load models at the consumer level. The process of creating the synthetic distribution system consists of locating and sizing distribution transformers, appropriately locating and sizing primary substations, and planning the low voltage system/secondaries and medium voltage system/primaries. The synthetic distribution network, used in this study, was validated by comparing characteristic metrics, statistically, against actual feeders from several U.S. utilities. The system was further validated by performing operational validation of the power flow and comparing synthetic voltage profiles with voltage profiles from real system data.

The synthetic distribution grid, used in this study, is a synthetic version of the Houston distribution system, in Texas, United States, including the counties of Harris, Chambers, Galveston, Brazoria, Waller Fortbend, and Montgomery. The system was created using the strategy described in previous work [37]. The main characteristics of this distribution grid are shown in Table II.

TABLE II:
Houston Distribution Case Parameters

Attribute	Value
Number of Customers	3,717,955
Number of Substations	710
Number of Feeders	2,303
Line Length (km)	117,393
Number of Lines	3,562,838
Area (km ²)	36,016
Active Power (MW)	16,749
Reactive Power (MVar)	3,518
Number of Generators	183
Number of Capacitors	3,195
Number of Transformers	738,223

B. Transmission System

The transmission system connected to the previously discussed distribution grid is created using the strategy outlined in [55]. This strategy details the assignment of substations, transmission lines and reactive power control devices, in three steps of substation planning, transmission planning and reactive power planning. These synthetic grids are validated based on characteristics of actual grids, used as validation metrics [56], [57], for achieving realistic data sets. The synthetic Texas grid, used in this study, is available at [58]. This grid is created based on publicly available data such as U.S. Census data [59] and generators' information that is available at the Energy Information Administration website [60]. Table III shows the important characteristics of the Texas transmission network that will be integrated with the distribution grid for this case study.

C. Transportation Data

TDMs are obtained from the Houston-Galveston Area Council [61]. For every EV trip, a Bayesian Network model trained on the Houston's Commercial Vehicle Survey is used to predict vehicle and trip attributes as a function of origin

TABLE III:
Texas Synthetic Transmission Grid Overview

Attribute	Value
Buses	6,717
Substations	4,894
Areas	8
Transmission lines	7,173
Transformers	1,967
Loads	5,095
Generators	731
Shunts	634
Peak load (GW)	75

county, arrival hour, and vehicle class [29]. Also, we use 2020 model year trip counts and vehicle miles traveled transportation data.

D. Scenarios

The combined transmission and distribution grid is studied in two interesting scenarios, for the purposes of this study, based on historical load data, in Texas. In addition, weather data containing wind speed, wind direction, cloud coverage and temperatures of the same days are directly included in the scenario to calculate the actual possible output of renewable generators. The two interesting scenarios are:

- Scenario 1: a day with high load and low availability of wind and solar (August 6, 2021)
- Scenario 2: a day with low load and high availability of wind and solar (October 16, 2021)

The twenty-four hour period of both of these scenarios is used, for the simulations. The generated time series data for both days was simulated, while solving the power-flow at each time step, with no added EV charging demand, to establish a base system. Additionally, the base case was simulated without the integrated co-simulation to see the differences between the separated and combined systems. The system was then simulated using two EV penetration cases:

- EV Penetration 1: 20% LD EV and 10% MHD EV
- EV Penetration 2: 30% LD EV and 20% MHD EV

Figures 3 and 4 show the overall demand of the base case in both scenarios before adding EV charging demand. Figure 3 shows the overall demand for the entire Texas transmission system over a 24-hour period, while Fig.4 shows the aggregated distribution load over a 24-hour period in Houston, TX specifically. These figures illustrate the difference between the high-load and low-load scenarios at the transmission and distribution levels. The calculated required charging demand from both LD and MHD EVs with the two EV penetration levels are shown in Fig. 5. This demand is then added to the base load of Scenarios 1 and 2 for simulation. Figures 6 and 7 show the locations and amount of aggregated LD and MHD EV charging loads in a sample 24 hours respectively, for scenario 1 and Penetration level 2. The color of these figures refers to the size of the load at each substation with darker colors referring to larger load. It is observed that LD EV load is lower compared to MHD EVs at each charging station but the number of LD EV fleets is higher.

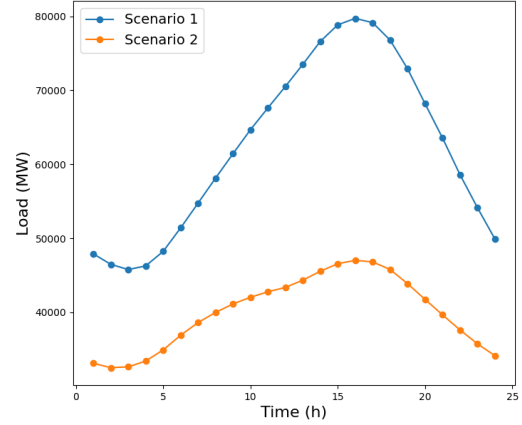


Fig. 3: Total base demand for Texas transmission grid

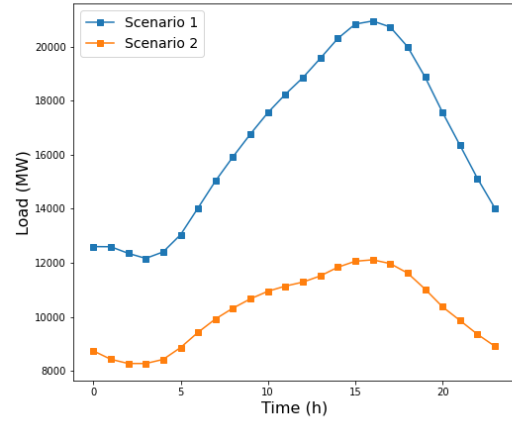


Fig. 4: Total base demand for Houston distribution grid

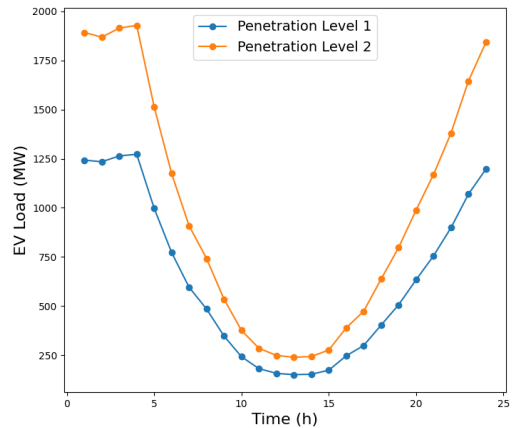


Fig. 5: EV charging demand for Houston distribution grid at different integration levels

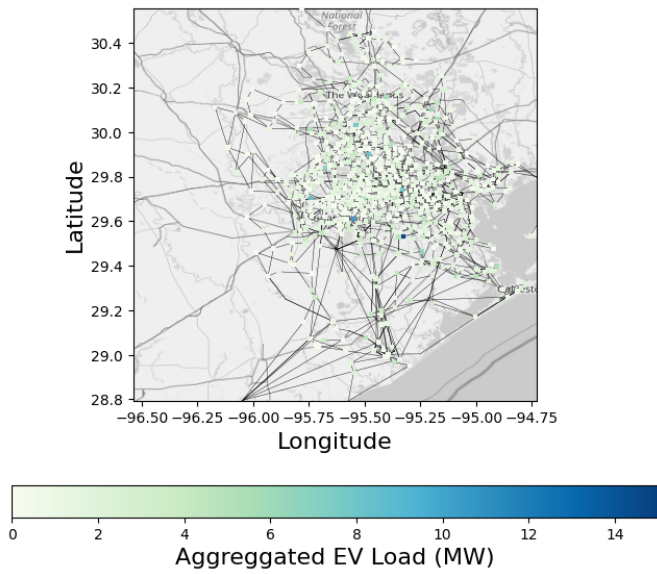


Fig. 6: Locations and amount of aggregated LD EV loads in a sample day using scenario 1 penetration level 2

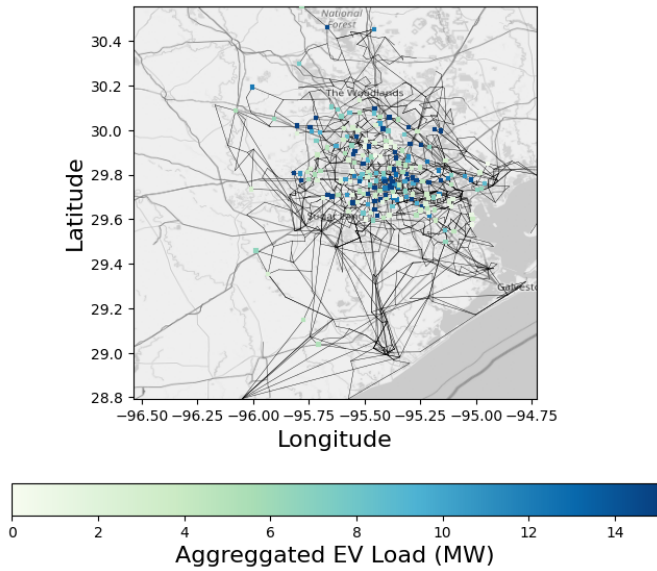


Fig. 7: Locations and amount of aggregated MHD EV loads in a sample day using scenario 1 penetration level 2

V. RESULTS AND DISCUSSION

A. Coordination Impact

To show the importance of the coordination strategy, the base case for Scenario 1 was simulated both as independent systems and coordinated systems. When comparing the independent transmission system simulation with the coordinated co-simulation, line loading for the independent transmission case is generally higher across the system. This can be seen in Fig. 8 where the difference in the co-simulation line-loading is shown in its relation to the transmission-only line-loading map, with the variation from the co-simulation illustrated by

the associated color map. Additionally, the variation in voltage, at transmission level buses, of the independent transmission simulation, when compared to the co-simulation is shown in Fig. 9.

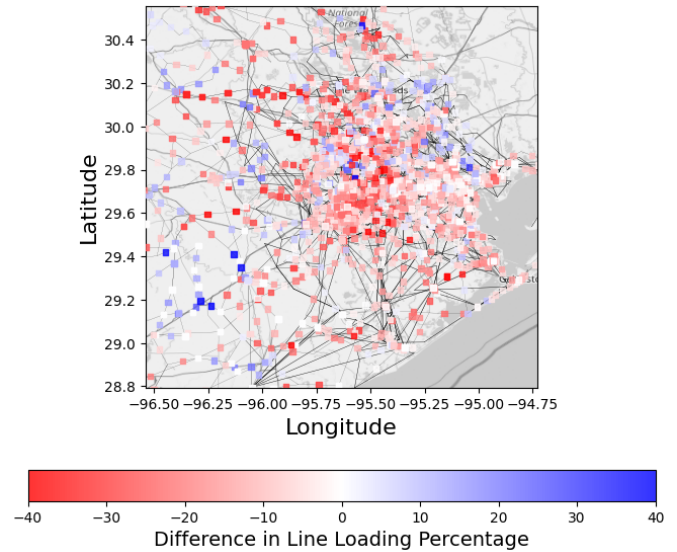


Fig. 8: Difference in line loading of the co-simulation from the independent transmission simulation

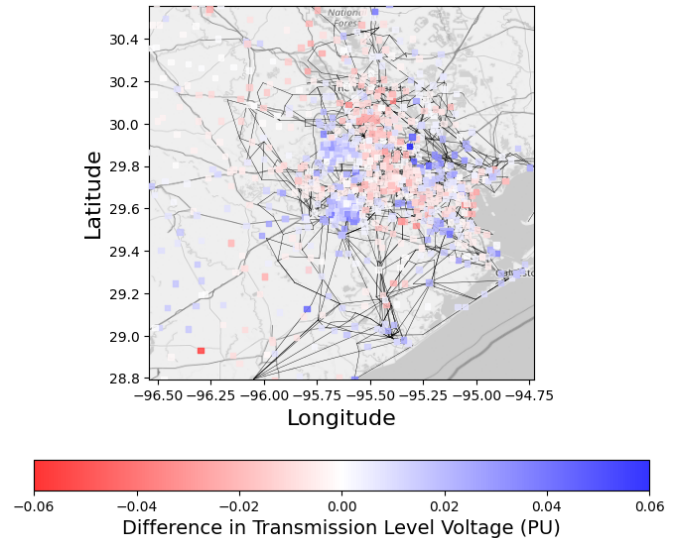


Fig. 9: Difference in voltage of the co-simulation from the independent transmission simulation

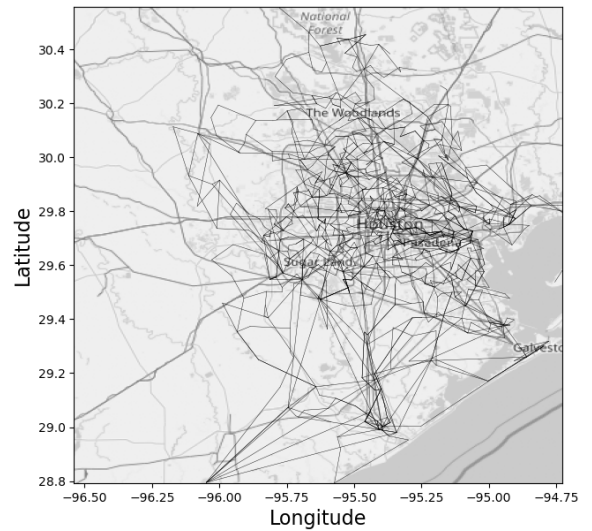
When comparing the independent distribution simulation with the co-simulation, the most variation in results was found in the reactive power distribution of the two systems. The reactive power throughout the system was generally higher in the independent distribution simulation compared to the co-simulation. However, the results of the independent system is not realistic, and shared values are forced from the distribution system to the transmission grid.

B. Weather Impacts

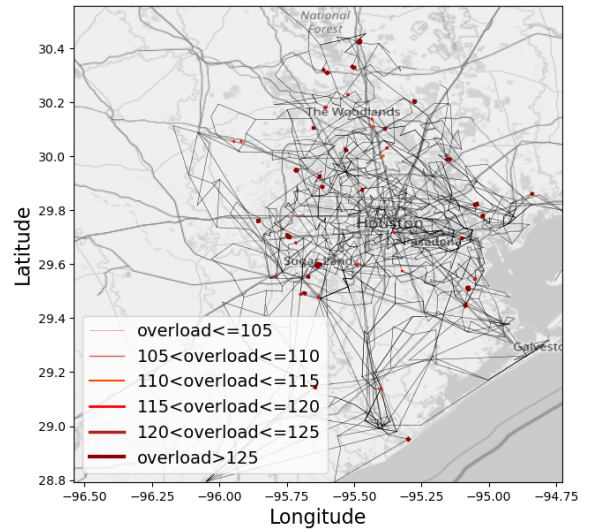
For the co-simulation scenarios, we show the importance of the direct inclusion of weather measurements, such as wind speed and cloud coverage, on the renewable generator capacities to solve a more precise ac OPF. To show the impact of weather measurements in the OPF, we ran the simulation, on the base case, with and without including weather data. The results show that the inclusion of weather data increased the LMP to \$34.54 compared to ac OPF results without including weather \$20.15. This is because the studied day, in scenario 1, is a high-load, low-wind day, and when ignoring the direct impact of the weather measurements, in the ac OPF results, it is assumed that wind turbines and solar cells can generate up to their nominal capacities when needed. However, as mentioned in our previous work [10] the available capacities of wind turbines and solar cells are dependent on the availability of these resources, and the weather measurements should be directly included in the calculations. Also, comparing distribution system line overloads for Scenario 1, with and without weather data, the results showed that including weather affects a higher degree of line overloads associated with EV charging demand. The overloaded lines for Scenario 1 Penetration Level 2, on the distribution level, at 3:00 AM, are shown in Figures 10a, 10b and 10c. Figure 10a shows that the base distribution case, without EV charging loads, for scenario 1 has no overloaded lines. Fig. 10b shows overloaded lines in a case with assumed high renewable generation, and Penetration level 1 EV charging loads. Fig. 10c shows the overloaded lines in the case with actual weather data added alongside Penetration level 1 EV charging loads. Therefore, including the direct impact of weather measurements in the power flow studies can change the available capacities and results significantly.

C. Scenario Impacts

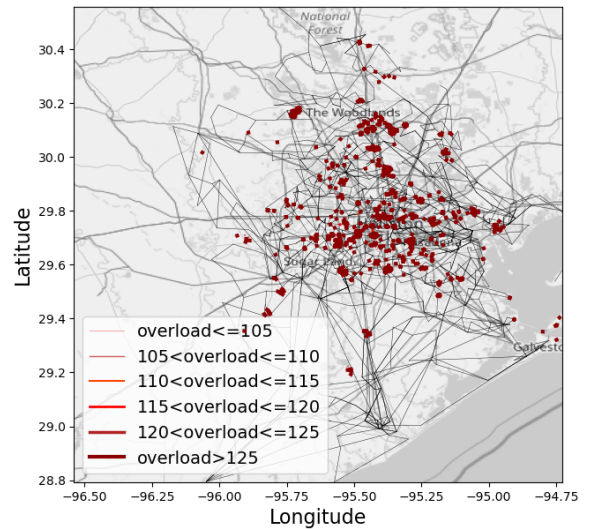
Weather and load scenarios 1 and 2 with EV penetrations 1 and 2 were also studied on the coordinated system. Figures 11a, and 11b show the substation load for scenarios 1 and 2 at 11:00 pm with penetration level 1. These two load maps show that Scenarios 1 and 2 were chosen for the study to represent two extremes of system loading, a high load day with low renewable availability contrasted with a low load day with high renewable availability. The load is illustrated using a color map based on load with units of kW. The predicted EV charging demand for both studied penetration levels is shown in Fig 5. The peak of EV charging demand is between 10:00 pm and 3:00 am, due to a concentration of most LD vehicles charging overnight. However, the overall distribution system suffers from a more significant strain between 1:00 pm and 3:00 pm, consistent with the peak of the base load. As expected an increase in load is seen in the system at certain substations in accordance with charging demand. This increase is illustrated in Figs 11a and 11b.



(a)



(b)



(c)

Fig. 10: Overloaded lines due to EV Charging in EV penetration level 1, scenario 1, at 3:00 AM, (a) without EV charging or weather impact (b) with EV and (c) with EV and direct inclusion of weather

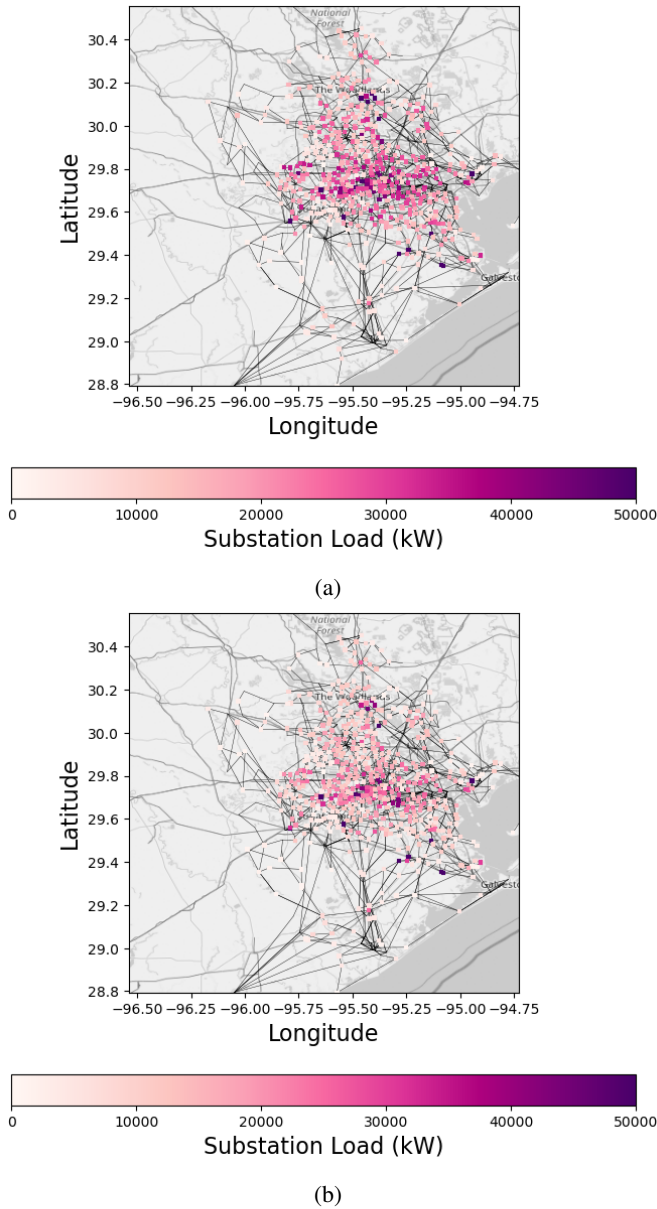


Fig. 11: Substation Load in Houston time series simulation (a) Scenario 1 penetration level 1 (b) Scenario 2 penetration level 1 at 11:00 pm

D. Discussion

A summary of changes to the distribution system caused by the increase in charging demand leading to system violations is shown in Table IV for each scenario and penetration level. The table also gives an overview of the magnitude of the highest overloaded lines, when in the study the highest overload occurred, the duration of the extreme overloads for each scenario and the hour for each scenario that has the highest number of overloaded lines in the distribution network as well as the number of overloaded lines.

As can be seen from the results, the current power grid is not ready to handle an integrated EV market and will require

TABLE IV: Overview of Violations and Overloads

Scenario	Scenario 1	Scenario 1	Scenario 2	Scenario 2
EV Penetration	Penetration 1	Penetration 2	Penetration 1	Penetration 2
Line Overloads	14896	19788	4893	6091
Transformer Overloads	11392	15489	3506	4318
Hour with worst Overloads	1:00 AM	3:00 AM	3:00 AM	3:00 AM
Overloads of Worst Hour	3297	5608	1529	2287
Highest Overload	245.7%	332.6%	260.9%	379.7%
Voltage Violations	108	107	192	190
Percentage of Overloads	0.42%	0.56%	0.14%	0.17%

upgrading to be able to handle significant EV integration. In fact, although the simulation did not cause a blackout, the duration and intensity of the overloads suffered in the system far exceeded the acceptable limits given by NERC and ANSI shown in Table I, which indicates the need for system upgrades.

E. Suggested System Upgrades

Table IV shows the number of line and transformer overloads voltage violations. From the results, it is clear that upgrades to the power system are necessary to avoid overloading and voltage issues caused by EV charging demand. The recommended upgrades include upgrading distribution lines, adding new lines, upgrading transformers, and adding switched shunts to areas that experience significant voltage fluctuations.

Under the charging conditions studied, we found that overall 18,438 distribution feeder lines needed to be upgraded to increase their capacities and an additional 1,350 lines needed to be added in parallel as shown in Table V. During the simulated charging event, these lines experienced overloads that exceeded the NERC established emergency limits set for the simulation [40], [41]. These upgraded lines compensate for the increased current demands of the EV charging, throughout the system. In addition to the line overloads, 15,489 transformers on distribution feeders were significantly overloaded. This would cause damage and on some of the significantly overloaded feeders blow out the transformer. To mitigate these overloads throughout the system, the line rating of each overloaded line is increased to the required rating to avoid overloads of the ratings mentioned in Table I so that the grid can safely handle the overloading current. If the overloads are above the highest distribution line rating capacities, then the limit of standard available line capacities [62] is reached and appropriately rated lines are added in parallel until the system is able to handle the line loading without limit violations. In a similar fashion the kVA ratings of overloaded transformers was increased until there was no longer a threat of overloading the transformer.

The locations of the necessary transformer and line upgrades are shown in Fig. 12 with the upgraded Transformers shown

TABLE V: Distribution System Required Line and Transformer Upgrades

Element	Line	Transformer
Overloads in EV Scenario	19788	15489
Percentage of Elements Overloaded	0.56%	9%
Upgraded System Elements	18438	15489
Required New Lines	1350	0

TABLE VI: Voltage Violation Mitigation

Voltage Violations Pre-Upgrades	New Capacitors Added	Feeder Voltage Violations Post-Upgrades
192	197	0

in green and upgraded lines shown, in red, and zoomed in, for clarity.

Also, bus voltage issues in the system are dealt with by adding switched shunts with the capability of injecting positive or negative reactive power. If the feeder voltage is low (for this work we considered lower than 0.9 pu), positive kVAR injection is needed so capacitive shunts are added. If the voltage is higher than the acceptable range (for this work considering 1.1 pu), negative reactive power injection is required so inductive shunts should be added. For this case, since voltage violations were lower than the acceptable range, it is required to add capacitors at locations with a low voltage issue. The voltage profile of the system during EV charging scenario 1, displaying these violations, is shown in Fig. 13. These voltages outside the acceptable range were mitigated, strategically, by placing new capacitors, within the system, in areas of high or low voltage violations. Table VI shows the number of required capacitors to be added to the system to avoid voltage issues and Fig. 14 shows their placement. When these capacitors are in place the voltage profile of the system improves to that shown in Fig. 15. The number of blocks and overall required capacity for each suggested capacitor bank is determined by finding the closest block size, available in [63] that provided enough kVAR capacity to bring the voltages, at a given substation, within acceptable limits. The step sizes for the capacitor banks is selected 100 kVAR which is available in industrial capacitors [63]. The required reactive power injection needed to stabilize the voltage at each feeder is calculated using equation (8).

VI. CONCLUSIONS

In this paper, an estimation of charging patterns of LD and MHD EVs based on actual transportation data was proposed and modeled. Then, the demand caused by the required EV charging based on EV type was mapped to a realistic distribution and transmission network at predicted times of day at different EV penetration levels on a variety of load and weather scenarios including a high demand, low renewable availability day, and a low demand, high renewable availabil-

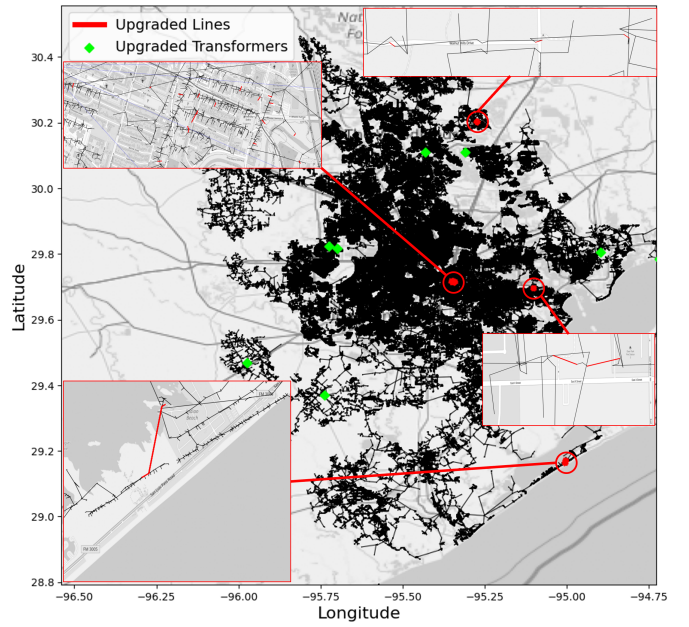


Fig. 12: Distribution transformers and lines that need to be upgraded to mitigate overloaded lines

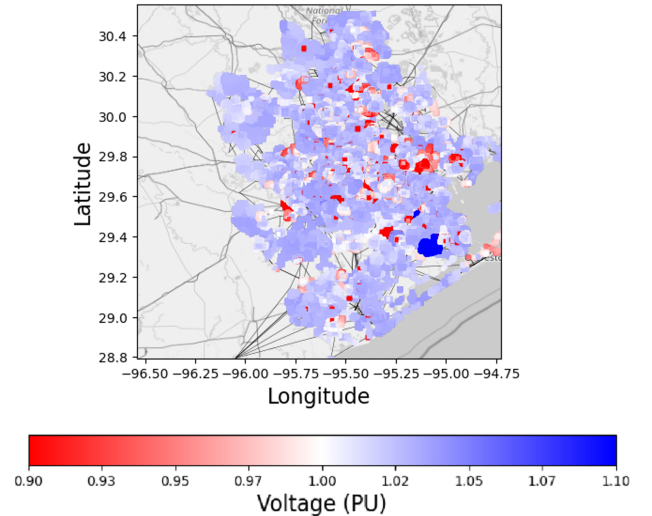


Fig. 13: Voltage map of distribution level substations in Houston pre-upgrades

ity day. The impact of weather measurement inclusion and added EV charging demand on a coordinated distribution and transmission system, was studied and the resulting overloads and voltage violations were analyzed, alongside changes in LMPs.

The study showed that including weather measurements and an increase in EV charging demand would lead to system overloads within the current electrical grid that exceeds the range and duration considered a safe operation. To avoid such issues, we recommended system upgrades such as adding distribution lines and reactive power control devices. In future

REFERENCES

- [1] "Electric Vehicle Outlook 2021". [Online]. Available: <https://about.bnef.com/electric-vehicle-outlook/>
- [2] "Global car sales estimates". [Online]. Available: <https://canalys.com/newsroom/canalys-global-electric-vehicle-sales-2020>
- [3] "Advanced Clean Cars II Regulations Resolution 22-12". [Online]. Available: <https://ww2.arb.ca.gov/sites/default/files/barcu/board/books/2022/082522/prores22-12.pdf>
- [4] L. Spangher, W. Gorman, G. Bauer, Y. Xu, and C. Atkinson, "Quantifying the impact of us electric vehicle sales on light-duty vehicle fleet co2 emissions using a novel agent-based simulation," *Transportation Research Part D: Transport and Environment*, vol. 72, pp. 358–377, 2019.
- [5] C. Ledna, M. Muratori, A. Yip, P. Jadun, and C. Hoehne, "Decarbonizing medium- & heavy-duty on-road vehicles: zero-emission vehicles cost analysis," National Renewable Energy Lab.(NREL), Golden, CO (United States), Tech. Rep., 2022.
- [6] P. Kluschke, T. Gnann, P. Plötz, and M. Wietschel, "Market diffusion of alternative fuels and powertrains in heavy-duty vehicles: A literature review," *Energy Reports*, vol. 5, pp. 1010–1024, 2019.
- [7] [Online]. Available: <https://www.epa.gov/newsreleases/biden-harris-administration-proposes-strongest-ever-pollution-standards-cars-and>
- [8] F. Safdarian, M. Ardehali, and G. Gharehpetian, "Ramp rate effect on maximizing profit of a microgrid using gravitational search algorithm," in *Proceedings of The IAJC-ISAM International Conference*, 2014.
- [9] J. Cao, W. Du, and H. Wang, "Weather-based optimal power flow with wind farms integration," *IEEE Transactions on Power Systems*, vol. 31, no. 4, pp. 3073–3081, 2015.
- [10] T. J. Overbye, F. Safdarian, W. Trinh, Z. Mao, J. Snodgrass, and J. H. Yeo, "An approach for the direct inclusion of weather information in the power flow," *Proc. 56th Hawaii International Conference on System Sciences (HICSS)*, 2023.
- [11] W. Su, J. Wang, K. Zhang, and M.-Y. Chow, "Framework for investigating the impact of phev charging on power distribution system and transportation network," in *IECON 2012-38th Annual Conference on IEEE Industrial Electronics Society*. IEEE, 2012, pp. 4735–4740.
- [12] J. Xiong, K. Zhang, Y. Guo, and W. Su, "Investigate the impacts of pev charging facilities on integrated electric distribution system and electrified transportation system," *IEEE Transactions on Transportation Electrification*, vol. 1, no. 2, pp. 178–187, 2015.
- [13] W. Wang, X. Fang, H. Cui, F. Li, Y. Liu, and T. J. Overbye, "Transmission-and-distribution dynamic co-simulation framework for distributed energy resource frequency response," *IEEE Transactions on Smart Grid*, 2021.
- [14] Y. Liu, T. J. Overbye, W. Wang, X. Fang, J. Wang, H. Cui, and F. Li, "Transmission-distribution dynamic co-simulation of electric vehicles providing grid frequency response," *2022 IEEE PES General Meeting*, pp. 1–5, 2022.
- [15] S. F. Abdelsamad, W. G. Morsi, and T. S. Sidhu, "On the impact of transportation electrification on distribution systems in the presence of rooftop solar photovoltaic," in *2015 IEEE Electrical Power and Energy Conference (EPEC)*. IEEE, 2015, pp. 26–31.
- [16] S. F. Abdelsamad, W. G. Morsi, and T. Sidhu, "Probabilistic impact of transportation electrification on the loss-of-life of distribution transformers in the presence of rooftop solar photovoltaic," *IEEE Transactions on Sustainable Energy*, vol. 6, no. 4, pp. 1565–1573, 2015.
- [17] J. Xiong, K. Zhang, X. Liu, and W. Su, "Investigating the impact of plug-in electric vehicle charging on power distribution systems with the integrated modeling and simulation of transportation network," in *2014 IEEE Conference and Expo Transportation Electrification Asia-Pacific (ITEC Asia-Pacific)*. IEEE, 2014, pp. 1–5.
- [18] M. Z. Zeb, K. Imran, A. Khattak, A. K. Janjua, A. Pal, M. Nadeem, J. Zhang, and S. Khan, "Optimal placement of electric vehicle charging stations in the active distribution network," *IEEE Access*, vol. 8, pp. 68 124–68 134, 2020.
- [19] D. Mao, J. Wang, J. Tan, G. Liu, Y. Xu, and J. Li, "Location planning of fast charging station considering its impact on the power grid assets," in *2019 IEEE Transportation Electrification Conference and Expo (ITEC)*. IEEE, 2019, pp. 1–5.
- [20] A. M. Farid, "Symmetrica: Test case for transportation electrification research," *Infrastructure Complexity*, vol. 2, no. 1, pp. 1–10, 2015.

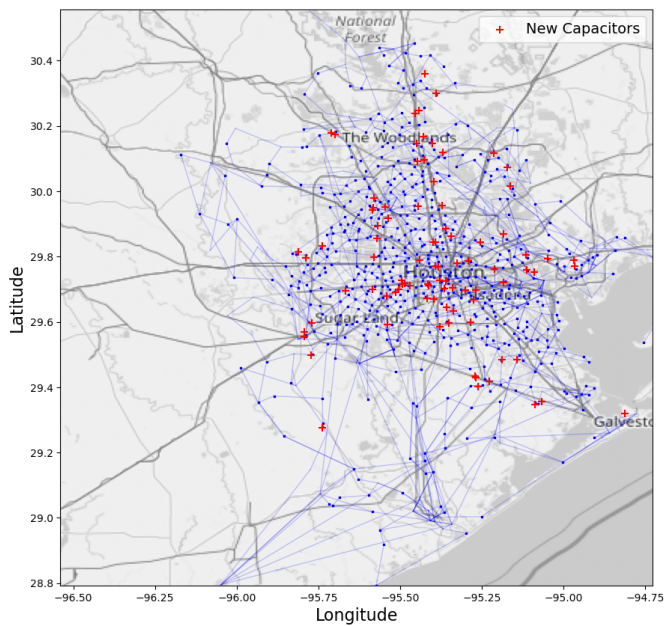


Fig. 14: Distribution capacitors that need to be added to mitigate voltage violations

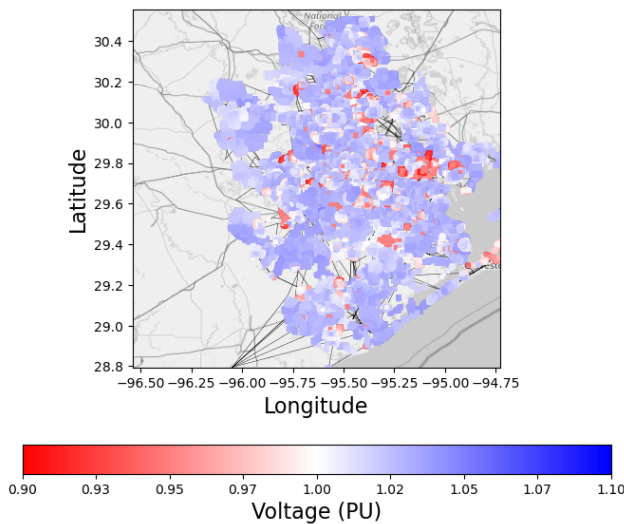


Fig. 15: System voltage profile after new capacitor integration

work, we will study the impact of weather scenarios on the transportation and other electric grid components such as transmission line impedances. Also, we model vehicle-to-grid and study its impact on the system's reliability and resiliency.

ACKNOWLEDGMENT

This work is partially supported through funding provided by the U.S. National Science Foundation (NSF) in Award 1916142, the U.S. ARPA-E Grant No. DE-AR0001366, and the Power Systems Engineering Research Center (PSERC).

- [21] M. Muratori, "Impact of uncoordinated plug-in electric vehicle charging on residential power demand," *Nature Energy*, vol. 3, no. 3, pp. 193–201, 2018.
- [22] K. S. Shetye, H. Li, J. L. Wert, X. Xu, A. Meitiv, Y. Xu, and T. J. Overbye, "Generation dispatch and power grid emission impacts of transportation electrification," in *2021 North American Power Symposium (NAPS)*. IEEE, 2021, pp. 01–06.
- [23] J. L. Wert, F. Safdarian, D. Wallison, J. K. Jung, Y. Liu, T. J. Overbye, and Y. Xu, "Spatiotemporal operational emissions associated with light-, medium-, and heavy-duty transportation electrification," *IEEE Transactions on Transportation Electrification*, 2023.
- [24] B. Borlaug, M. Muratori, M. Gilleran, D. Woody, W. Muston, T. Canada, A. Ingram, H. Gresham, and C. McQueen, "Heavy-duty truck electrification and the impacts of depot charging on electricity distribution systems," *Nature Energy*, vol. 6, no. 6, pp. 673–682, 2021.
- [25] S. Farnsworth, J. Bauer, and L. Larsen, "2010 houston-galveston area council commercial vehicle survey technical summary," Texas Department of Transportation, Tech. Rep., 2013. [Online]. Available: <https://ftp.dot.state.tx.us/pub/txdot-info/tp/survey/houston-2010-commercial.pdf>
- [26] X. Xu, H. A. Aziz, H. Liu, M. O. Rodgers, and R. Guensler, "A scalable energy modeling framework for electric vehicles in regional transportation networks," *Applied Energy*, vol. 269, p. 115095, 2020.
- [27] Y. Wang and D. Infield, "Markov chain monte carlo simulation of electric vehicle use for network integration studies," *International Journal of Electrical Power & Energy Systems*, vol. 99, pp. 85–94, 2018.
- [28] X. Xu, H. A. Aziz, H. Liu, M. O. Rodgers, and R. Guensler, "A scalable energy modeling framework for electric vehicles in regional transportation networks," *Applied Energy*, vol. 269, p. 115095, 2020.
- [29] A. Meitiv, "Commercial vehicle trip generator based on the houston-galveston area council survey," *CARTEEH DATA:HUB*, 2021. [Online]. Available: <http://carteehdata.org/library/dataset/commercial-vehicle-trip-g-94c7>(accessedFeb012022)
- [30] D. Pevec, J. Babic, A. Carvalho, Y. Ghiassi-Farrokhfal, W. Ketter, and V. Podobnik, "A survey-based assessment of how existing and potential electric vehicle owners perceive range anxiety," *Journal of Cleaner Production*, vol. 276, p. 122779, 2020. [Online]. Available: <https://www.sciencedirect.com/science/article/pii/S0959652620328249>
- [31] J. Smart and S. Schey, "Battery electric vehicle driving and charging behavior observed early in the ev project," *SAE International Journal of Alternative Powertrains*, vol. 1, no. 1, pp. 27–33, 2012.
- [32] Q. Xing, Z. Chen, Z. Zhang, X. Xu, T. Zhang, X. Huang, and H. Wang, "Urban electric vehicle fast-charging demand forecasting model based on data-driven approach and human decision-making behavior," *Energies*, vol. 13, no. 6, p. 1412, 2020.
- [33] C. G. Chorus, "A new model of random regret minimization," *European Journal of Transport and Infrastructure Research*, vol. 10, no. 2, 2010.
- [34] D. E. Bell, "Regret in decision making under uncertainty," *Operations research*, vol. 30, no. 5, pp. 961–981, 1982.
- [35] L. Spangher, W. Gorman, G. Bauer, Y. Xu, and C. Atkinson, "Quantifying the impact of us electric vehicle sales on light-duty vehicle fleet co2 emissions using a novel agent-based simulation," *Transportation Research Part D: Transport and Environment*, vol. 72, pp. 358–377, 2019.
- [36] J. L. Wert, K. S. Shetye, H. Li, J. H. Yeo, X. Xu, A. Meitiv, Y. Xu, and T. J. Overbye, "Coupled infrastructure simulation of electric grid and transportation networks," in *2021 IEEE Power & Energy Society Innovative Smart Grid Technologies Conference (ISGT)*, 2021.
- [37] H. Li, J. L. Wert, A. B. Birchfield, T. J. Overbye, T. G. S. Roman, C. M. Domingo, F. E. P. Marcos, P. D. Martinez, T. Elgindy, and B. Palmintier, "Building highly detailed synthetic electric grid data sets for combined transmission and distribution systems," *IEEE Open Access Journal of Power and Energy*, vol. 7, pp. 478–488, 2020.
- [38] H. Li, J. H. Yeo, A. L. Bornsheuer, and T. J. Overbye, "The creation and validation of load time series for synthetic electric power systems," *IEEE Transactions on Power Systems*, vol. 36, no. 2, pp. 961–969, 2021.
- [39] A. Wood, B. Wollenberg, and G. Sheblé, *Power Generation, Operation, and Control*. Wiley, 2013. [Online]. Available: <https://books.google.com/books?id=JDVmAQAQBAJ>
- [40] "System operating limit definition and exceedance clarification," North American Electric Reliability Corporation (NERC), Tech. Rep., January 2015. [Online]. Available: https://www.nerc.com/pa/comp/guidance/EROEndorsedImplementationGuidance/System_Operating_Limit_definition_and_Exceedance_Clarification_endorsed.pdf
- [41] "Capacity rating procedures," ISO New England (ISO-NE), Tech. Rep., October 2004. [Online]. Available: https://www.iso-ne.com/static-assets/documents/rules_proceds/isone_plan/pp07/capacity_rating_procedures.pdf
- [42] "Weather Station Identifiers". [Online]. Available: <http://www.weathergraphics.com/identifiers/>
- [43] "Current Weather and Wind Station Data". [Online]. Available: https://aviationweather.gov/adds/dataserver_current/current/metars.cache.csv
- [44] "ERA5 hourly data on single levels from 1940 to present". [Online]. Available: <https://cds.climate.copernicus.eu/cdsapp#!/dataset/reanalysis-era5-single-levels?tab=form>
- [45] (2021) "U.S. Energy Information Administration (EIA)". [Online]. Available: <https://www.eia.gov/electricity/data/eia860/>
- [46] G. M. Masters, *Renewable and efficient electric power systems*. John Wiley & Sons, 2013.
- [47] V. Sohoni, S. Gupta, R. Nema *et al.*, "A critical review on wind turbine power curve modelling techniques and their applications in wind based energy systems," *Journal of Energy*, vol. 2016, 2016.
- [48] C. Draxl, A. Clifton, B.-M. Hodge, and J. McCaa, "The wind integration national dataset (wind) toolkit," *Applied Energy*, vol. 151, pp. 355–366, 2015.
- [49] P. Giorsetto and K. F. Utsurogi, "Development of a new procedure for reliability modeling of wind turbine generators," *IEEE Transactions on Power Apparatus and Systems*, no. 1, pp. 134–143, 1983.
- [50] A. De Sa and S. Al Zubaiby, "Gas turbine performance at varying ambient temperature," *Applied Thermal Engineering*, vol. 31, no. 14–15, pp. 2735–2739, 2011.
- [51] J. L. Wert, T. Chen, F. Safdarian, J. Snodgrass, and T. J. Overbye, "Calculation and Validation of Weather-Informed Renewable Generator Capacities in the Identification of Renewable Resource Droughts," in *IEEE PowerTech 2023*, 2023.
- [52] F. Safdarian, J. Cook, S. J. Lee, and T. J. Overbye, "Calculation and validation of weather-informed renewable generation in the us based on era5 hourly weather measurements," in *IEEE Power and Energy Conference at Illinois (PECI) 2024*. IEEE, 2024, pp. 1–6.
- [53] "End-Use Load Profiles for the U.S. Building Stock: Market Needs, Use Cases, and Data Gaps". [Online]. Available: <https://www.osti.gov/biblio/1576489/>
- [54] "End Use Load Profiles for the U.S. Building Stock". [Online]. Available: <https://comstock.nrel.gov/datasets>
- [55] K. M. Gegner, A. B. Birchfield, T. Xu, K. S. Shetye, and T. J. Overbye, "A methodology for the creation of geographically realistic synthetic power flow models," in *2016 IEEE Power and Energy Conference at Illinois (PECI)*, 2016, pp. 1–6.
- [56] V. Krishnan, B. Bugbee, T. Elgindy, C. Mateo, P. Duenas, F. Postigo, J.-S. Lacroix, T. G. S. Roman, and B. Palmintier, "Validation of synthetic u.s. electric power distribution system data sets," *IEEE Transactions on Smart Grid*, vol. 11, no. 5, pp. 4477–4489, 2020.
- [57] A. B. Birchfield, E. Schweitzer, M. H. Athari, T. Xu, T. J. Overbye, A. Scaglione, and Z. Wang, "A metric-based validation process to assess the realism of synthetic power grids," *Energies*, vol. 10, no. 8, 2017. [Online]. Available: <https://www.mdpi.com/1996-1073/10/8/1233>
- [58] Texas A&M University Electric Grid Datasets, 2019. [Online]. Available: <https://electricgrids.engr.tamu.edu/>
- [59] "Census 2019, zip code tabulation areas gazetteer file." 2019. [Online]. Available: <https://www.census.gov/geo/maps-data/data/gazetteer2019.html>
- [60] U.S. Energy Information Administration (EIA) form 860, 2019. [Online]. Available: <http://www.eia.gov/electricity/data/eia860/index.html>
- [61] Houston-Galveston Area Council, "Regional travel models: 2016 model validation and documentation report," Houston-Galveston Area Council, Tech. Rep., March 2019.
- [62] "Ampacity Chart". [Online]. Available: <https://www.cityelectricsupply.com/electricreferences>
- [63] [Online]. Available: <https://www.eaton.com/content/dam/eaton/products/medium-voltage-power-distribution-control-systems/power-capacitors/capacitor-block-banks-and-accessories-catalog-ca230009en.pdf>